BBA - Gene Regulatory Mechanisms 1866 (2023) 194889

Contents lists available at ScienceDirect

BBA - Gene Regulatory Mechanisms

journal homepage: www.elsevier.com/locate/bbagrm

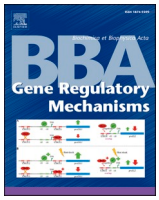

EP400NL is involved in *PD-L1* gene activation by forming a transcriptional coactivator complex

Zidong Li [a], Hyoungmin Kim [b], Jaehoon Kim [b], Jeong Hyeon Park [a,c,*]

[a] School of Natural Sciences, Massey University, Palmerston North 4442, New Zealand
[b] Department of Biological Sciences, Korea Advanced Institute of Science and Technology, Daejeon 34141, South Korea
[c] Department of Biological Sciences, Xi'an Jiaotong-Liverpool University, Suzhou, Jiangsu 215123, China

ARTICLE INFO

Keywords:
Cancer
Chromatin remodelling
cMyc
PD-L1
H2A.Z
Epigenetic

ABSTRACT

EP400 is an ATP-dependent chromatin remodelling enzyme that regulates DNA double-strand break repair and transcription, including cMyc-dependent gene expression. We previously showed that the N-terminal domain of EP400 increases the efficacy of chemotherapeutic drugs against cancer cells. As the *EP400 N-terminal-Like* (*EP400NL*) gene resides next to the *EP400* gene locus, this prompted us to investigate whether EP400NL plays a similar role in transcriptional regulation to the full-length EP400 protein. We found that EP400NL forms a human NuA4-like chromatin remodelling complex that lacks both the TIP60 histone acetyltransferase and EP400 ATPase. However, this EP400NL complex displays H2A.Z deposition activity on a chromatin template comparable to the human NuA4 complex, suggesting another associated ATPase such as BRG1 or RuvBL1/RuvBL2 catalyses the reaction. We demonstrated that the transcriptional coactivator function of EP400NL is required for serum and IFNγ-induced *PD-L1* gene activation. Furthermore, transcriptome analysis indicates that EP400NL contributes to cMyc-responsive mitochondrial biogenesis. Taken together, our studies show that EP400NL plays a role as a transcription coactivator of *PD-L1* gene regulation and provides a potential target to modulate cMyc functions in cancer therapy.

1. Introduction

The E1A binding protein P400 (EP400) ATPase is one of the subunits of human NuA4 (hNuA4) histone acetyltransferase (HAT) complex that regulates transcription through chromatin remodelling of target genes [1,2]. In addition to EP400, the hNuA4 complex consists of over 16 subunits including the phosphatidylinositol 3-kinase family protein kinase homolog TRRAP (Transformation/transcription domain-associated protein), the HAT TIP60, and bromodomain-containing BRD8 [2]. EP400 catalyses ATP-dependent H2A.Z deposition to regulate gene expression and DNA double-strand break repair [3,4]. The TIP60-less EP400 complex, a variant of hNuA4 complex, also promotes histone variant H3.3 deposition at target gene loci, suggesting that EP400-mediated histone variant (H2A.Z/H3.3) deposition activity could play a key role in the epigenetic regulation of these genes [5,6]. In connection, the global transcription amplifier cMyc recruits the hNuA4 complex, and its interactions with TRRAP and EP400 are required for cMyc-mediated gene activation [7–9].

One of the genes regulated by cMyc is programmed death ligand-1 (*PD-L1*), which is required for immune checkpoint control [10,11]. The ligand-receptor interaction between PD-L1 and PD-1 has been extensively studied as a target of cancer immunotherapy ever since it was implicated in the suppression of cytotoxic T lymphocytes and immune tolerance [12]. cMyc has been demonstrated to bind to the *PD-L1* gene promoter to induce expression, however, the molecular mechanisms through which this occurs are not well understood [13,14]. In addition to cMyc-mediated PD-L1 expression, the pro-inflammatory cytokine interferon-gamma (IFNγ) also induces PD-L1 expression in a variety of tumours including melanoma, non-small cell lung cancer (NSCLC), and renal cell carcinoma [15–17]. This phenomenon has been referred to as innate immune resistance, which is a survival strategy of tumor cells to escape immune surveillance [18–20].

We previously showed that expression of N-terminal domain of EP400 (1–719 amino acid residues) increases the efficacy of chemotherapeutic drugs against U2OS cancer cells [21]. Interestingly, the *EP400 N-terminal-Like* (*EP400NL*) gene resides next to *EP400* on chromosome 12q24.33. The N-terminal 131–490 amino acid residues of EP400 share 92 % sequence similarity over 84.5 % of the full-length

* Corresponding author at: Department of Biological Sciences, Xi'an Jiaotong-Liverpool University, Suzhou, Jiangsu 215123, China.
E-mail addresses: hm.kim@kaist.ac.kr (H. Kim), kimjaehoon@kaist.edu (J. Kim), Jeong.Park@xjtlu.edu.cn (J.H. Park).

https://doi.org/10.1016/j.bbagrm.2022.194889
Received 30 July 2022; Received in revised form 19 October 2022; Accepted 24 October 2022
Available online 31 October 2022

EP400NL polypeptide. Despite no previous identification of any functional domains and its subsequent annotation as a pseudogene, *EP400NL* appears to be regulated by an independent promoter, and the exon regions are highly conserved across many vertebrates (UCSC genome browser). Given their adjacent genetic location and sequence similarity, we hypothesized that EP400NL may have a regulatory function distinct from its paralog EP400 in the regulation of EP400-target genes. Here, we report that EP400NL forms a unique nuclear complex distinct from the EP400 chromatin remodelling complex and serves as a transcriptional coactivator in serum and IFNγ-stimulated *PD-L1* transcriptional activation.

2. Materials and methods

2.1. Mammalian cell culture

Unless specified, cells were maintained in Dulbecco's Modified Eagle's Medium (DMEM, Gibco/Life Technologies) supplemented with 5 % fetal bovine serum (FBS) and 0.5 % Penicillin-Streptomycin and 5 % CO_2. For serum starvation, cells were grown for 48 h in the DMEM medium containing 1 % FBS and then stimulated with 20 % FBS. IFNγ was used at 5 ng/ml for IFNγ stimulation (Carlsbad, CA 92008, USA).

2.2. Generation of EP400NL indel mutation by CRISPR/Cas9

EP400NL targeted guide RNA (AGGTTGTGGCCAGAAAGCAC), luciferase targeted guide RNA (AACGCCTTGATTGACAAGGA), and scrambled guide RNA (AAACATGTATAACCCTGCGC) were used to produce indel mutations according to the procedure using eSpCas9-LentiCRISPR,v2, (Genscript, Hong Kong, China) [22].

2.3. Purification and elution of EP400NL complex

Flp-In™ T-REx™ cell line that stably expresses EP400NL was generated using the Flp-In™ T-Rex™ System (Invitrogen). Flp-In™T-REx™ cells are HEK293T cells with a stably integrated flip recombination target (FRT) site. EP400NL was cloned into the pcDNA5/FRT/TO expression vector and then co-transfected with pOG44 DNA expressing Flp recombinase. The transfected cells were treated with 30 μg/ml of hygromycin and the resistant colonies were screened by checking the tetracycline-inducible expression of EP400NL. The resultant Flp-In T-Rex monoclonal cells were fractionated after tetracycline induction according to the Dignam and Roeder nuclear extraction method [23]. Briefly, approximately 5×10^8 cells of tetracycline-induced Flp-In T-Rex cell line were harvested and prepared for a nuclear soluble fraction. The fraction was subjected to gel filtration chromatography using Bio-Gel A1.5 resin equilibrated with streptavidin binding buffer (10 mM Tris, pH 8.0, 150 mM NaCl, 2 mM EDTA pH 8.0, 0.1 % NP40, and 10 mM 2-Mercaptoethanol). TAP-EP400NL protein, tagged with both streptavidin-binding peptide (SBP) and calmodulin-binding peptide (CBP) was affinity-purified by using streptavidin-conjugated agarose beads (EZview™ Red Streptavidin Affinity Gel, Sigma-Aldrich).

2.4. Histone acetyltransferase assay

A plasmid containing 16 repeats of 601-Widom nucleosome positioning sequences (pUC19/601 × 16) was utilized for generating multi-nucleosomes using Hela-free histones. 2 × HAT buffer (40 mM Tris pH 9.0, 100 mM KCl, 1 mM EDTA, 10 mM DTT, 20 mM sodium butyrate, 10 % glycerol), 1 μg of the assembled chromatin, and immunoprecipitated proteins were initially incubated for 10 min at 30 °C, followed by the addition of [^{14}C]-Acetyl-coenzyme A (0.02 μCi), and incubated for another 1 h at 30 °C. The reactions were inactivated by the addition of 6 μl of 6 × SDS sample buffer. Samples were boiled at 90 °C for 5 min before 10–15 % SDS-PAGE analysis. Proteins were transferred onto a membrane blot and immediately stained with Ponceau S for detecting histone proteins. Membranes were air-dried in the air circulating safe cabinet overnight and exposed to Biomax MS film at −80 °C for 5 days for radioactive signal exposure.

2.5. H2A.Z deposition assay

A plasmid containing 16 repeats of 601-Widom nucleosome positioning sequences (pUC19/601 × 16) was used to assemble the chromatin substrate. Biotin labelling of the nucleosome assembly was conducted using the EZ-Link™ Psoralen-PEG3-Biotin kit (Thermo Scientific™) according to the manufacturer's instructions. The partially purified enzyme fractions were added to the reaction mixture containing 100 ng FLAG-H2A.Z/H2B dimer, 500 ng assembled chromatin, 1× protease inhibitor (Roche), and 1 mM ATP and incubated for 1 h at 30 °C. The chromatin was harvested by the streptavidin-conjugated agarose beads (EZview™ Red Streptavidin Affinity Gel, Sigma-Aldrich), and analysed by immunoblotting.

2.6. Dual-luciferase reporter assays

HEK293TGal4-Luciferase cells were seeded in 24-well plates and transfected with CbF-Gal4Myc (20 ng), pRenilla-CMV (1 ng), and plasmids expressing various cofactors (200 ng) using Effectene transfection reagent (QIAGEN). After 48 h, firefly luciferase and renilla luciferase activities were measured using the Dual-Luciferase® Reporter Assay System (Promega). Experiments were conducted in triplicate and averaged firefly luciferase activity was normalized to the corresponding Renilla activity.

2.7. Confocal microscopy

Cells were seeded in a 6-well plate at a density of 1.5×10^5 cells/ml and grown on UV sterilised coverslips. Cells were processed according to manufacturer's instructions (R&D Systems: rndsystems.com/IHCProtocol) and imaged on a Zeiss LSM900 confocal laser scanning microscope.

2.8. Quantitative reverse transcription-PCR (RT-qPCR)

Total RNA was purified using Trizol according to the manufacturer's instruction (R2070 including DNaseI digestion step, Zymo Research, Australia) and the quantity and quality (A_{260}/A_{280}) of purified RNA were assessed by Nanodrop spectrophotometer. The primer pairs of GUSB (beta-glucuronidase, reference gene) and PD-L1 were obtained from a commercial source (QuantiTect primer assay, GUSB: QT00046046; PD-L1: QT00082775, Qiagen). Triplicate samples of 4 μl from total RNA preparations were analysed using SensiFAST SYBR No-Rox One-Step Kit (Bioline, Australia) [0.2 μM forward and reverse primers, 12.5 μl of enzyme reaction mixture, 0.2 μl of reverse transcriptase and Taq DNA polymerase mixture]. PCR was performed at 45 °C for 30 min for cDNA synthesis and followed by conventional quantitative PCR (95 °C for 5 s and 60 °C for 30 s, 40 cycles) on a Roche Lightcycler 480. Serially diluted RNA samples were used to generate a standard curve for both GUSB and PD-L1 using the average of Cp values versus log [1/dilution factor]. The correlation coefficient r between Cp and log [relative abundance] on a standard curve was used as a PCR quality control. The relative expression levels of PD-L1 were determined by normalising against the expression levels of GUSB.

2.9. Chromatin immunoprecipitation-quantitative PCR (ChIP-qPCR) assays

Chromatin immunoprecipitation (ChIP) assays were performed according to the Abcam high-sensitivity ChIP kit (ab185913, Abcam). The antibodies and primer information [24,25] are summarised in supplementary tables 1 and 2.

2.10. Transcriptome analysis

For RNA sequencing, the expression of TAP-tagged EP400NL in the Flp-In™ T-Rex™ cell line was induced by 1 μM tetracycline treatment in normal growth medium for 12 h and RNA was manually extracted with Trizol. Library was prepared with TruSeq Stranded Total RNA with Ribo-Zero H/M/R_Gold (Illumina) and sequenced with the Illumina NovaSeq platform. For RNA sequencing analysis, the adaptors were trimmed with Trimmomatic [26]. STAR, featurecount, DESeq2 were used for alignment, gene quantification, and analysis of differential gene expression [27–29]. In DEseq2, *p*-value was determined with Benjamini-Hochberg method. cMyc target genes were retrieved from Public RNA-seq data (accession number: GSE164926) [30] and compared with the EP400NL-upregulated genes.

2.11. Statistical analysis

Statistical analysis was performed using GraphPad Prism software version 8.0 (GraphPad Software Inc., San Diego, CA, USA). Data were compared with either a one-way or two-way ANOVA statistical test depending on the experimental design and followed by either Dunnett's multiple comparisons, Tukey's multiple comparisons, or Sidak's multiple comparisons as appropriate and indicated in the text. All data shown were determined from independent experiments and presented as the mean ± SD.

3. Results

3.1. EP400NL forms a nuclear complex distinct from the EP400 chromatin remodelling complex

To identify EP400NL-associated proteins, the Flp-In™ T-Rex™ stable cell line was generated to inducibly express TAP-tagged EP400NL in a tetracycline-dependent manner (Supplementary Fig. 1). Inducible expression of the TAP-tagged EP400NL and endogenous EP400NL was confirmed by immunoblotting (Fig. 1A). To characterise the subcellular distribution, cytosolic, soluble nuclear, and insoluble nuclear fractions were analysed by immunoblotting and showed that EP400NL was predominantly detected in the soluble nuclear fraction (Fig. 1B, left panel). The nuclear localisation of tetracycline-induced TAP-EP400NL was further verified by confocal microscopy on cells co-labelled with DAPI (Fig. 1B, right panel).

To identify EP400NL-associated proteins, TAP-tagged EP400NL complex was isolated from the soluble nuclear fraction of the tetracycline-induced cell line by a combination of size exclusion chromatography and SBP affinity tag purification. The purified protein complexes were then resolved by SDS-PAGE and identified by mass spectrometry (Fig. 1C). Not surprisingly, most of the identified proteins were integral components of hNuA4 chromatin remodelling complexes including BRD8, BAF53, DMAP1, RuvBL2 (TIP48), MRGBP, and YEATS4 [2,31].

Consistent with the results obtained from the mass spectrometry, FLAG-tagged EP400NL that was transiently expressed in HEK293T cells co-immunoprecipitated with BRG1, BRD8, BAF53, and RuvBL2 (Fig. 1D). FLAG-tagged EP400NL also appears to be associated with the endogenous EP400, albeit with an insignificant level (Fig. 1D, lane 6 of EP400 blot). Given the transient overexpression condition, the weak EP400 signal observed in the co-immunoprecipitation reaction is likely due to the nonspecific mass action that does not occur in the Flp-In™ T-Rex™ stable cell line used in the purification process. RuvBL1 (TIP49) is known to form a hetero-oligomeric complex with RuvBL2 in most human nuclear complexes [32]. Although RuvBL1 was not identified by the mass spectrometry, it was confirmed to interact with EP400NL by co-immunoprecipitation. Interestingly, BRG1, a core ATPase subunit of the human SWI/SNF chromatin remodelling complexes, was identified as a component of the EP400NL-associated proteins by the mass spectrometry and further confirmed by co-immunoprecipitation (Fig. 1D, α-BRG1 blot, lane 6). BRG1 has not been reported as a component of the hNuA4 complex [1,2,31], however, it does associate with EP400NL. It is also associated with FLAG-tagged DMAP1 but not FLAG-tagged TIP60 in the co-immunoprecipitation assay (Fig. 1D, α-BRG1 blot, lanes 6, 7 versus 8). Proteins bound to FLAG-tagged EP400NL, -DMAP1, and -TIP60 were partially purified respectively under native conditions by FLAG peptide elution (Fig. 1E, left panel, α-FLAG blot). The HAT assay using ^{14}C-labelled acetyl coenzyme A and chromatin as substrates showed a lack of HAT activity from the EP400NL complex, suggesting that TIP60 or any other HAT is not associated with EP400NL or the HAT activity is suppressed within the EP400NL complex (Fig. 1E, right panel, ^{14}C–labelled histones, lane 2). The presence of BRG1 and the lack of detection of TRRAP, EP400, and HAT activities (Fig. 1) together indicate that EP400NL is a component of a nuclear complex that is distinct from the hNuA4 complex.

3.2. The EP400NL nuclear complex catalyses an H2A.Z deposition in chromatin in vitro

The identification of H2A.Z as an EP400NL-interacting protein by mass spectrometry (Fig. 1C) led us to investigate whether this complex mediates ATP-dependent H2A.Z deposition as previously shown by the EP400 complex [4,33]. FLAG-tagged H2A.Z/H2B dimers were used as a substrate to determine whether the purified FLAG-tagged EP400NL complex catalyses H2A.Z deposition into chromatin (Fig. 2A). As a positive control, the hNuA4 complex was purified from HeLa nuclear extract using FLAG-tagged TIP60, and the presence of each core protein (RuvBL1, RuvBL2, and BAF53) was confirmed by immunoblotting (Fig. 2B). Consistent with the mass spectrometry data, BRG1 was found in the EP400NL complex but not in the hNuA4 complex. Plasmids containing the 601-Widom nucleosome positioning repeats (pUC19/601 × 16) were biotinylated and used to generate synthetic chromatin with recombinant core histones (H2A, H2B, H3, and H4). Synthetic chromatin assemblies were validated by micrococcal nuclease (MNase) digestion that showed a 200-bp spaced ladder (Fig. 2C). In the presence of ATP, the EP400NL complex catalysed an increase in FLAG-H2A.Z deposition activity into chromatin 5-fold over background, as did the hNuA4 complex (Fig. 2D). This result, together with H2A.Z found in the purified EP400NL complex, suggests that the EP400NL complex has the potential to catalyse H2A.Z incorporation into chromatin in vivo and facilitate transcriptional activation.

3.3. EP400NL serves as a coactivator of GAL4Myc-mediated transcriptional activation

Given EP400NL forms a nuclear complex with subunits in common with the EP400 chromatin remodelling complex [7,34], the ability of EP400NL to act as a coactivator was tested. To that end, luciferase activity in 293TGal4-Luciferase cells [35,36] was determined in the presence of increasing ectopic expression of EP400NL (Fig. 3A). In the presence of a steady amount of the GAL4Myc transcription activator, a dose-dependent increase in luciferase activity of up to three-fold was observed (Fig. 3A, right panel), confirming that EP400NL acts as a coactivator of cMyc transactivation domain.

To demonstrate activator-dependent recruitment of EP400NL to target genes, chromatin immunoprecipitation (ChIP) was performed on 293TGal4-Luciferase cells in the presence or absence of ectopic FLAG-tagged GAL4Myc. A similar induction level of TAP-tagged EP400NL was confirmed by immunoblot analysis (Fig. 3B). The enrichment of EP400NL at the GAL4 binding site was significantly increased by approximately 8-fold in the presence of GAL4Myc, indicating that the recruitment of EP400NL is dependent on GAL4Myc (Fig. 3C). As expected, neither GAL4Myc nor EP400NL was enriched in the distal exon region of *p21*. Taken together, these results suggest that EP400NL is recruited to the promoter to activate gene expression in a DNA-binding

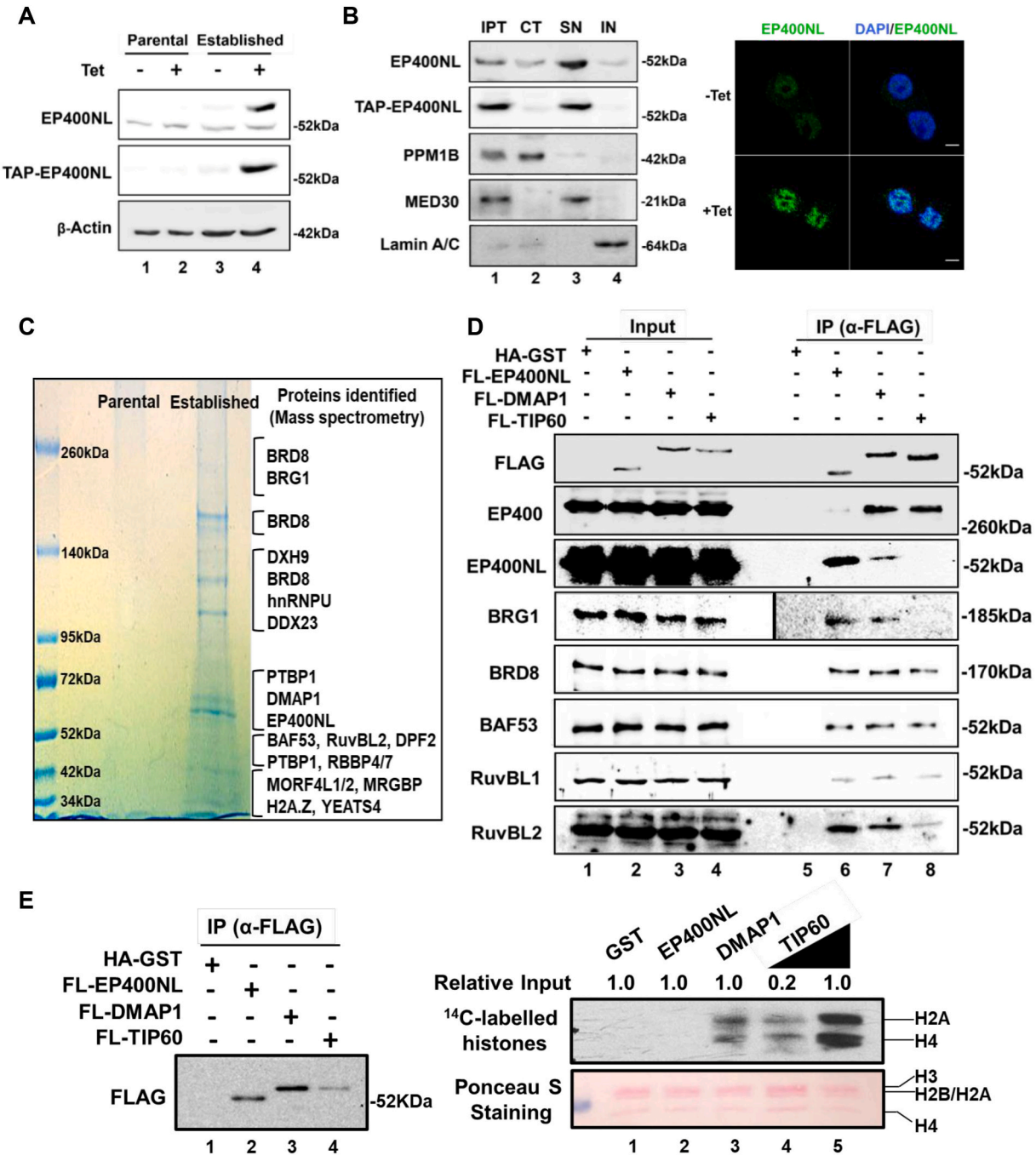

Fig. 1. EP400NL forms a nuclear complex similar to the EP400 chromatin remodelling complex.
(A) Immunoblot analysis of lysates from HEK293 Flp-In™ T-Rex™ cells stably transfected with tetracycline-inducible TAP-tagged EP400NL. TAP-tagged EP400NL (60 KDa in molecular mass) and endogenous EP400NL (52 kDa in molecular mass) are shown by anti-EP400NL and anti-CBP TAP-tag immunoblots. (B) Cellular fractionation of EP400NL. Input control (IPT), cytosolic fraction (CT), soluble nuclear fraction (SN), and insoluble nuclear pellet (IN) were analysed by immunoblotting (left panel). PPM1B, MED30, and Lamin A/C are used as the markers of cytosol, nucleoplasm, and an insoluble component of the nuclear pellet, respectively. The subcellular localization of TAP-EP400NL was analysed by immunocytochemistry with anti-EP400NL and counterstaining with DAPI (right panel). Scale bar = 10 μm. (C) Colloidal Coomassie Blue G250 staining of EP400NL nuclear complex. Proteins were purified from Flp-In™ T-Rex™ cell lines expressing TAP-EP400NL or the parental control, and resolved by SDS-PAGE. Excised gel slices were analysed by mass spectrometry and identified proteins are shown. (D) Interaction of EP400NL with the candidate proteins by co-immunoprecipitation. HEK293T cells were transiently transfected with plasmids expressing HA-GST, FLAG-EP400NL, FLAG-DMAP1, or FLAG-TIP60 and the cell lysates were immunoprecipitated with anti-FLAG antibody. The immunoprecipitates were analysed by immunoblotting using antibodies as indicated. A solid dividing line on the BRG1 blot indicates a conjoined image of two blots from a lower and higher exposure. (E) HAT assay of EP400NL nuclear complex. The amounts of partially purified FLAG-tagged EP400NL, -DMAP1, and -TIP60 after FLAG peptide elution were assessed by immunoblotting (left panel). Detection of the radioactively labelled histones catalysed by the associated HAT is shown (right panel). Equivalent loading of histone proteins was validated by Ponceau staining. (For interpretation of the references to colour in this figure legend, the reader is referred to the web version of this article.)

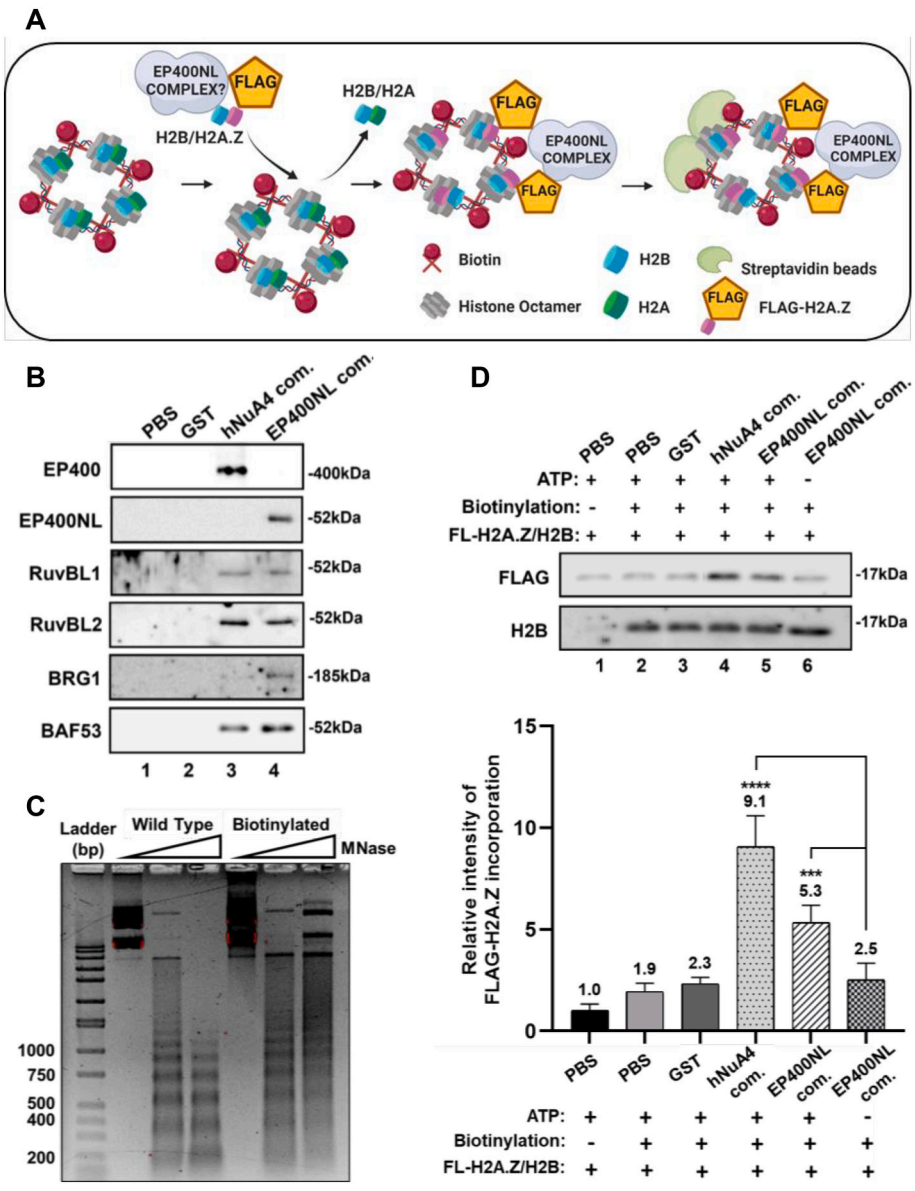

Fig. 2. EP400NL nuclear complex catalyses H2A.Z deposition activity in the chromatin in vitro.
(A) Schematic illustration of H2A.Z deposition assay. (B) Purified protein preparations used in the H2A.Z deposition assay were analysed by immunoblotting for the core components of the protein complexes including EP400, EP400NL, RuvBL1, RuvBL2, BRG1, and BAF53. (C) Micrococcal Nuclease (MNase) digestion assay of the assembled chromatin. Chromatin substrates assembled with either biotin-labelled pUC19/601 × 16 or unlabelled plasmid DNA were digested by two different concentrations of MNase (3.75×10^{-3} U (low); 1.5×10^{-2} U (high)) and analysed by 1 % agarose gel electrophoresis. (D) Detection of FLAG-H2A.Z incorporation into the chromatin substrate by immunoblotting. The reactions were resolved by SDS-PAGE and H2A.Z deposition activities were analysed by anti-FLAG immunoblot (top panel). The relative intensity of FLAG-H2A.Z was initially normalized to the H2B signals and the normalized value from the negative control (PBS and non-biotinylated chromatin) was set to one and the relative activities from other samples were plotted (bottom panel) [One-way ANOVA, $F_{(5,24)} = 65.75$, $p < 0.0001$; post-hoc Tukey's HSD, $^{***}p < 0.001$ (EP400NL + ATP Vs. EP400NL-ATP), $^{****}p < 0.0001$ (EP400 + ATP Vs. EP400NL-ATP)].

transcription factor-dependent manner.

No functional domains within EP400NL have been identified to date, however, the bioinformatics prediction tool InterPro was used to predict several potential functional regions within EP400NL (Fig. 3D). To investigate the importance of these regions in the interactions with BAF53, BRD8, and BRG1, full-length EP400NL and four deletion mutants of EP400NL were generated and transiently expressed in HEK293T cells (Fig. 3E). While all of the mutants retained the ability to interact with BAF53, BRD8 and BRG1, two deletion mutants of EP400NL (Δ246–260 and Δ360–419) showed a modest decrease in the interaction with BAF53 even at higher levels of ectopic expression than that of wild-type EP400NL (Fig. 3E). In addition, two EP400NL mutants (Δ1–50 and Δ360–419) appear to show an enhanced association with BRD8 compared to the wild-type and other EP400NL mutants. The deletion studies of EP400NL suggest that the distal ends of EP400NL play an important role in the interaction with BAF53 and BRD8, which would affect its transcriptional coactivator function.

To examine whether the mutants also retained coactivator activity, they were tested for their ability to co-activate GAL4Myc-mediated luciferase reporter expression. The Δ1–50 deletion mutant showed a modest increase in coactivator activity, whereas the deletion of either residues 246–260 or 360–419 resulted in the complete loss of coactivator activity compared to full-length EP400NL (Fig. 3F).

3.4. *EP400NL serves as a coactivator for both serum and IFNγ-induced PD-L1 gene activation*

Given that EP400NL was recruited to the promoter by the cMyc transactivation domain (Fig. 3C), a possible involvement of EP400NL in *PD-L1* gene regulation was explored since upregulation of PD-L1 is considered one of the critical therapeutic cMyc targets in cancer. Serum serves as a source of various growth hormones and growth factors. It is well-known to activate cMyc and stimulate cellular proliferation, both of which are correlated with PD-L1 expression [37,38]. TAP-EP400NL expression in Flp-In™ T-Rex™ cells resulted in a 3.2-fold increase in *PD-L1* mRNA in the presence of serum stimulation (Fig. 4A, Ser+/Tet+). Consistent with the effect on *PD-L1* mRNA level, PD-L1 protein increased 2-fold compared to the untreated cells (Fig. 4B).

As IFNγ increases PD-L1 expression in tumours [14–17], it was investigated whether EP400NL also enhances IFNγ-induced PD-L1 expression. IFNγ treatment alone increased *PD-L1* mRNA expression by approximately 2-fold and additional treatment of either serum or

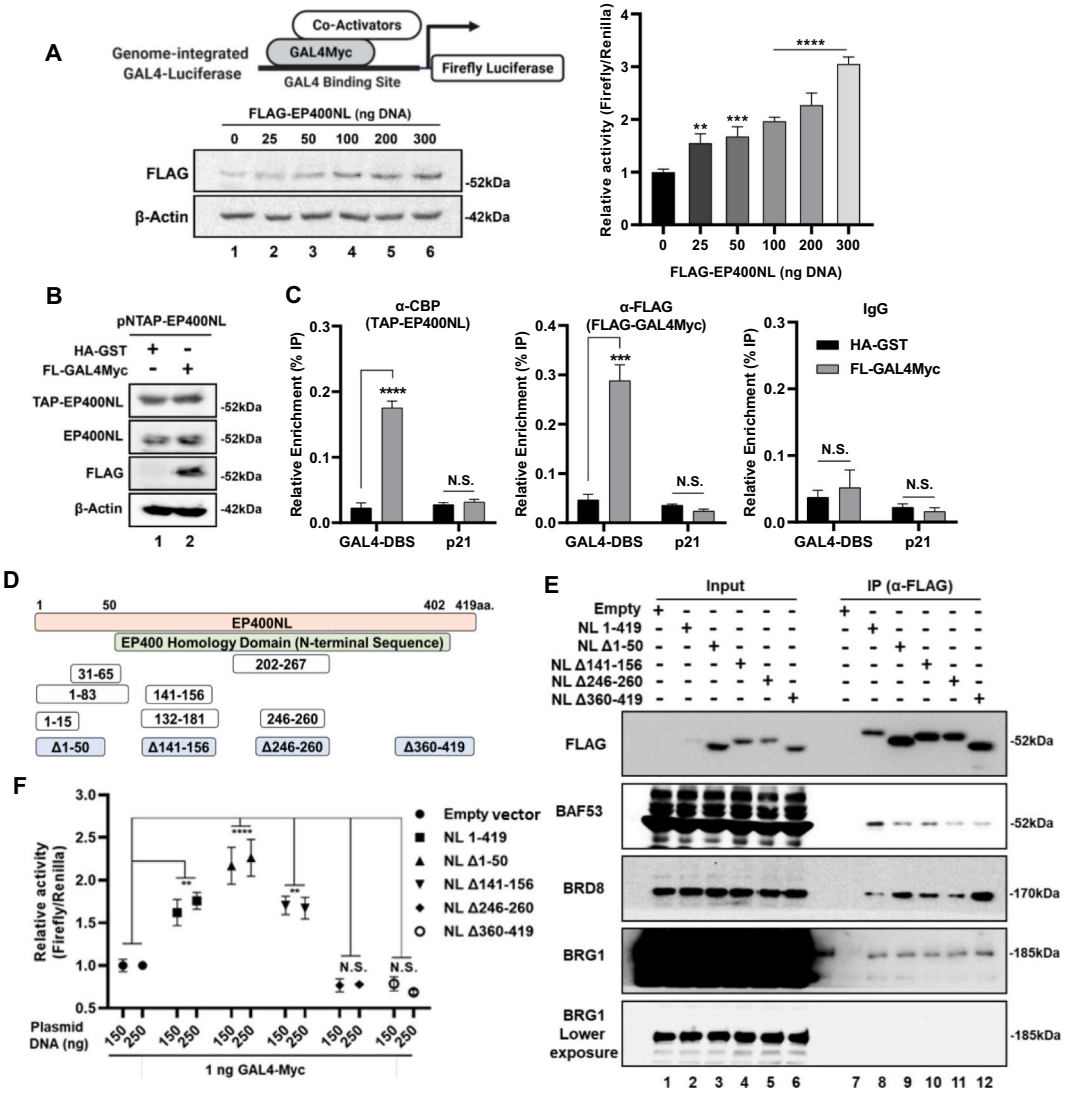

Fig. 3. EP400NL serves as a coactivator in GAL4Myc-mediated transcriptional activation.
(A) Titration of EP400NL expression in 293TGal4-Luciferase cells using firefly luciferase reporter assays. Expression of EP400NL was confirmed by anti-FLAG immunoblot (left panel) and the relative firefly luciferase activities were plotted against the amount of DNA used in the transfection (right panel). [One-way ANOVA, $F_{(5,12)} = 61.11$, $p < 0.0001$; Dunnett's post-hoc test, $^{**}p < 0.01$, $^{***}p < 0.001$, $^{****}p < 0.0001$] (B) 293TGal4-Luciferase cells were co-transfected with plasmids expressing either HA-GST (control) or FLAG-GAL4Myc together with TAP-EP400NL. Transgene expression before ChIP analyses was confirmed by immunoblotting. (C) ChIP analyses were performed using anti-CBP for TAP-tagged EP400NL (left), anti-FLAG for GAL4Myc (middle), and IgG as a negative control (right). GAL4-DBS (GAL4 DNA binding site), *p21* (*p21* distal exon region). [Two-way ANOVA, $F_{(1,4)} = 225.7$, $p = 0.0001$ (CBP), $F_{(1,4)} = 107.0$, $p = 0.0005$ (FLAG); Sidak's post-hoc test, $^{***}p < 0.001$, $^{****}p < 0.0001$]. (D) Schematic presentation of four deletion mutants of EP400NL. White boxes represent the seven predicted functional sites by the bioinformatic tool (InterPro). Four EP400NL deletion mutants (Δ1–50, Δ141–156, Δ246–260, and Δ360–419) were generated based on the InterPro prediction (blue boxes). (E) Co-immunoprecipitation assays of full-length FLAG-tagged EP400NL (NL 1–419) and deletion mutants. (F) Firefly luciferase reporter assays in 293TGal4-Luciferase cells. The cells were transfected with either 150 ng or 250 ng of plasmid DNA expressing full-length EP400NL or the deletion mutants together with 1 ng of Gal4Myc expression plasmid. [Two-way ANOVA, $F_{(5,24)} = 50.28$, $p < 0.0001$; post-hoc Tukey's HSD, $^{**}p < 0.01$, $^{****}p < 0.0001$]. (For interpretation of the references to colour in this figure legend, the reader is referred to the web version of this article.)

increased TAP-EP400NL resulted in an additive effect (Fig. 4C). Interestingly, *PD-L1* gene expression was synergistically upregulated up to 8-fold by triple treatments with IFNγ, serum, and TAP-EP400NL induction (Fig. 4C, IFNγ+/Serum+/Tet+). A similar pattern of PD-L1 protein expression was observed in the triple-treated cells with a 2.5-fold increase compared to the control cells (Fig. 4D).

To confirm the activation of *PD-L1*, Flp-In™ T-Rex™ cells were tetracycline-induced to express TAP-EP400NL in the presence and absence of serum and IFNγ treatment and then stained with anti-PD-L1 and anti-EP400NL antibodies, and DAPI for microscopic imaging. While increased EP400NL expression was detected after tetracycline induction, PD-L1 levels were unchanged in the absence of serum- or IFNγ stimulation (Fig. 4E and F, top two panels). However, all cells expressed a higher level of PD-L1 after serum or IFNγ stimulation, which was further increased after EP400NL induction (Fig. 4E and F, bottom two panels). Taken together, these results indicate that EP400NL requires simultaneous signals from serum or IFNγ treatment to exert its strong coactivator function in the activation of *PD-L1*.

In contrast to wild type EP400NL, neither deletion mutants (Δ246–260 and Δ360–419) enhanced the serum and IFNγ-stimulated expression of *PD-L1* mRNA (Fig. 4G) or protein (data not shown). These data confirm that the regions of EP400NL between amino acids 246–260 and 360–419 are critical for the EP400NL-mediated coactivator function.

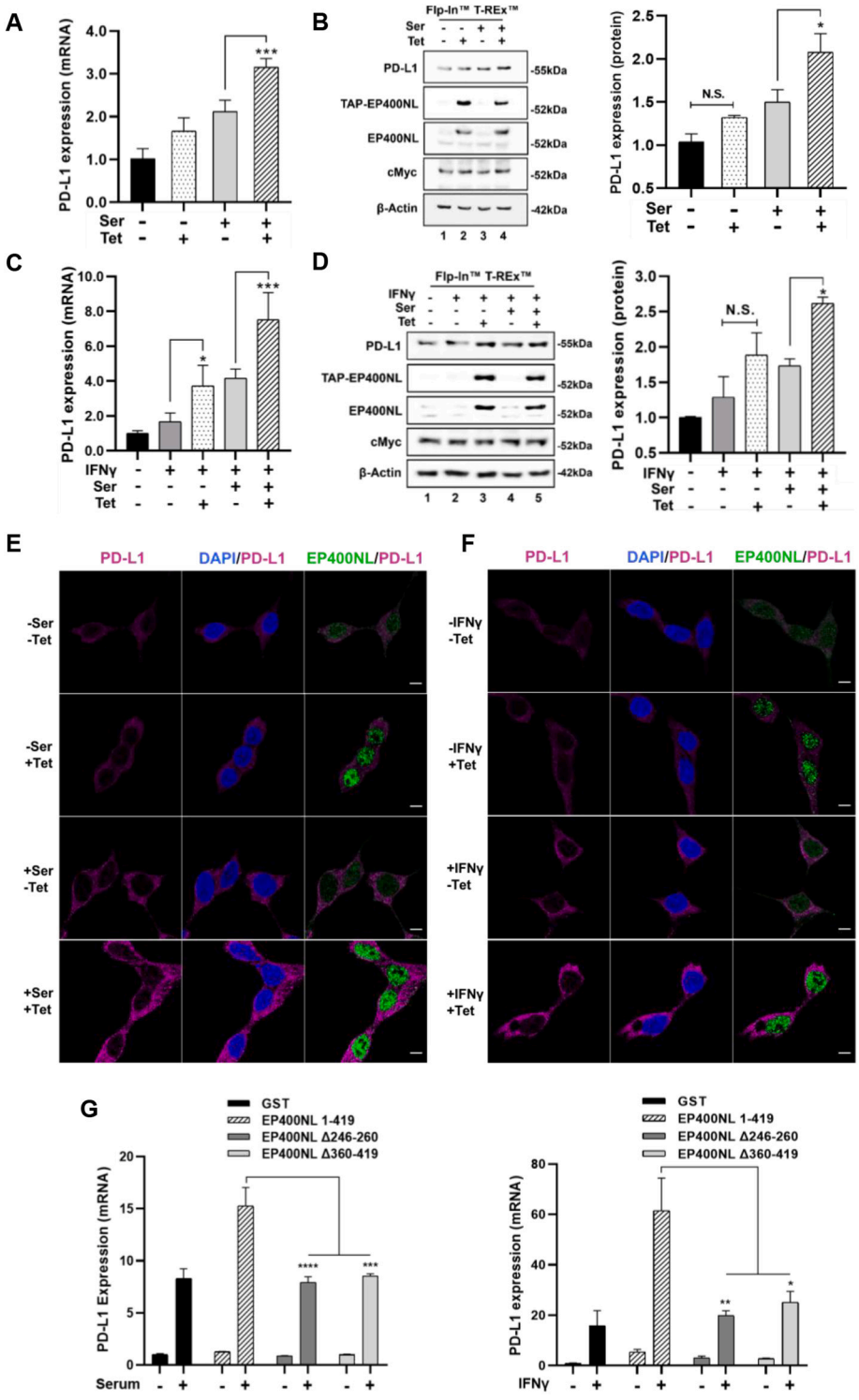

Fig. 4. EP400NL serves as a coactivator for both serum- and IFNγ-mediated PD-L1 gene activations. (A, C) *PD-L1* mRNA levels in response to tetracycline-induced EP400NL and either serum stimulation (A) or IFNγ treatment (C). Flp-In™ T-Rex™ cells were treated under four different conditions (±Ser/±Tet) and the total RNA of each treatment was analysed by RT-qPCR assays [One-way ANOVA, $F_{(3,12)} = 48.96$, $p < 0.0001$; post-hoc Tukey's HSD, $^{***}p < 0.001$]. (B, D) PD-L1 protein expression levels in response to tetracycline-induced EP400NL and either serum stimulation (B) or IFNγ treatment (D). [One-way ANOVA, $F_{(4,15)} = 30.42$, $p < 0.007$; post-hoc Tukey's HSD, $^{*}p < 0.05$, $^{***}p < 0.001$]. (E and F) Immunocytochemical analysis of PD-L1 in the TAP-EP400NL inducible Flp-In™ T-Rex™ cell line. Cells were treated with either a combination of serum stimulation and tetracycline induction (E) or a combination of IFNγ stimulation and tetracycline induction (F) followed by the staining with the anti-PD-L1 and anti-EP400NL antibodies. Nuclei were counterstained with DAPI. Scale bar = 5 μm. (G) EP400NL mutants lose the coactivator function for both serum- and IFNγ-mediated PD-L1 expression. H1299 cells were transiently transfected with plasmids expressing either full-length EP400NL (1–419) or two deletion mutants (Δ246–260 and Δ360–419). *PD-L1* mRNA levels induced by serum stimulation (left panel) or IFNγ stimulation (right panel) were determined by RT-qPCR assays [Two-way ANOVA, $F_{(3,8)} = 18.60$, $p = 0.0006$ (Serum stimulation). $F_{(3,8)} = 7.112$, $p = 0.012$ (IFNγ sensitization); post-hoc Tukey's HSD, $^{*}p < 0.05$, $^{**}p < 0.01$, $^{***}p < 0.001$, $^{****}p < 0.001$].

To further confirm the role of EP400NL in mediating serum- and IFNγ-mediated *PD-L1* gene activation, CRISPR/Cas9-mediated EP400NL indels were generated in H1299 cells. To confirm the presence of indels at the target sites, high-resolution melting peak analysis (HRM) was employed to examine melt peak shifting and relative fluorescent signal differences of the dissociation curves (Supplementary Fig. 2). Two-biological replicates of each EP400NL indel cell line show the alteration of genomic DNA at the intended deletion sites and significantly decreased protein expression of endogenous EP400NL (Fig. 5B and D, anti-EP400NL immunoblots). However, the targeted deletion of *EP400NL* did not completely abrogate the endogenous EP400NL protein, suggesting that a portion of the polyclonal cell population still expresses EP400NL.

To investigate if the downregulation of EP400NL can affect serum- and IFNγ-mediated PD-L1 expression, the two EP400NL indel lines (Indel-A, Indel-B) were used to examine PD-L1 expression over time following serum or IFNγ stimulation. H1299 control cells displayed a 100-fold increase in *PD-L1* mRNA after 6 h of serum stimulation, whereas the polyclonal EP400NL indel H1299 cells showed a compromised transcriptional induction profile with only a 30-fold increase at

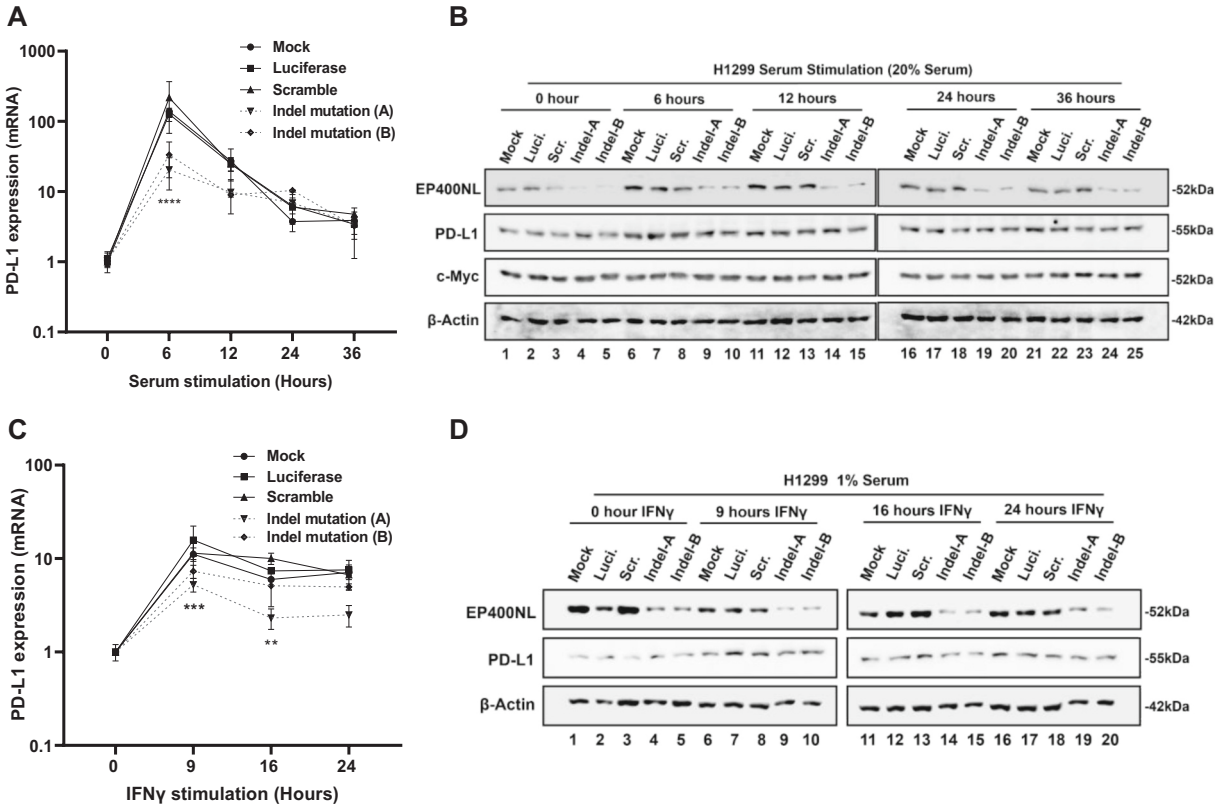

Fig. 5. EP400NL enhances both serum and IFNγ mediated PD-L1 expression.
(A and C) *PD-L1* mRNA expression levels in H1299 cell lines carrying EP400NL indels. These experiments were conducted under the condition of either serum stimulation (A) or IFNγ stimulation (C). The basal PD-L1 expression level of each cell line set to one and the expression levels of PD-L1 were calculated against their basal expression levels [Two-way ANOVA, $F_{(4,25)} = 21.10$, $p < 0.0001$ (Serum stimulation), $F_{(3,20)} = 36.56$, $p < 0.0001$ (IFNγ sensitization); post-hoc Tukey's HSD, $^{**}p < 0.001$ (Scr. versus Indel-A, IFNγ sensitization), $^{***}p < 0.001$ (Luci. Vs. Indel-A, IFNγ stimulation) $^{****}p < 0.0001$ (Scr. versus Indel-A or Indel-B, serum stimulation)]. (B and D) EP400NL immunoblots for H1299 cell lines established by CRISPR-Cas9 system: Mock, gRNA-luciferase (Luci.), gRNA-scrambled random sequence (Scr.), gRNA-EP400NL-A (Indel-A), and gRNA-EP400NL-B (Indel-B). Protein expression levels of endogenous PD-L1 under either serum stimulation (B) or IFNγ stimulation (D) were examined by immunoblotting, respectively.

the same time point (Fig. 5A). Similarly, IFNγ-induced PD-L1 expression was also decreased in the EP400NL indel cell lines, with a significantly lower expression level in one of the biological replicates (Indel-A) (Fig. 5C). Taken together, the loss of function studies using CRISPR/Cas9-mediated indels confirm the critical role of EP400NL in driving both serum and IFNγ-mediated *PD-L1* transcriptional activation. However, the weaker transcriptional activity of the *PD-L1* gene caused by EP400NL indels failed to show significant downregulation of PD-L1 protein by immunoblotting (Fig. 5B and D). Since PD-L1 expression is known to be regulated at multiple levels, including translational and post-translational regulations [19,39–45], the mechanism behind this discordance needs further investigation.

3.5. The EP400NL nuclear complex interacts with cMyc and binds to the PD-L1 promoter in a serum stimulation-dependent manner

It was next investigated as to whether the interaction of cMyc with EP400NL complex occurs under physiological conditions using the stable Flp-In T-Rex cell line. Following tetracycline induction and serum stimulation, TAP-EP400NL was immunoprecipitated and the presence of endogenous cMyc, BRG1, RuvBL1, and RuvBL2 was detected (Fig. 6A, lanes 6 and 8). The reverse immunoprecipitation using anti-cMyc, anti-BRG1, anti-RuvBL1, and anti-RuvBL2 antibodies resulted in immunoprecipitation of TAP-EP400NL (Fig. 6B, lanes 6, 8, 10, and 12). These results further support a hypothesis that cMyc directly interacts with the EP400NL nuclear complex containing BRG1, RuvBL1, and RuvBL2.

To examine whether EP400NL is recruited to the *PD-L1* promoter in a serum stimulation-dependent manner, ChIP was performed following induction of TAP-EP400NL expression in Flp-In™ T-Rex™ cells. Cells were serum-starved to maintain a low growth rate and then treated with high serum to promote cell growth. Despite serum stimulation, no significant increase of cMyc enrichment at the *PD-L1* promoter was detected, however, TAP-EP400NL induction enhanced cMyc enrichment upon serum stimulation (Fig. 7A, cMyc panel). BRG1 and RuvBL2 showed a similar recruitment pattern in which both serum stimulation and tetracycline induction of EP400NL resulted in a significantly higher enrichment than serum stimulation or EP400NL induction alone (Fig. 7A). These data indicate that cellular signals induced by serum stimulation are prerequisite for the enrichment of BRG1 and RuvBL2 ATPases near the cMyc binding site of the *PD-L1* gene, which can be significantly enhanced by EP400NL.

To determine whether the activation of *PD-L1* is associated with H2A.Z deposition at the *PD-L1* promoter in vivo, ChIP analysis was performed following serum and IFNγ stimulation (Fig. 7B). The result indicates that activation of the *PD-L1* promoter is accompanied by inducible increases in H2A.Z deposition where the EP400NL complex may contribute to the epigenetic alteration of the chromatin that leads to gene activation.

3.6. EP400NL plays a role in the gene regulation involved in mitochondrial biogenesis

To identify EP400NL-responsive genes, the transcriptional profile of the tetracycline-induced Flp-In T-Rex cell line was examined in the

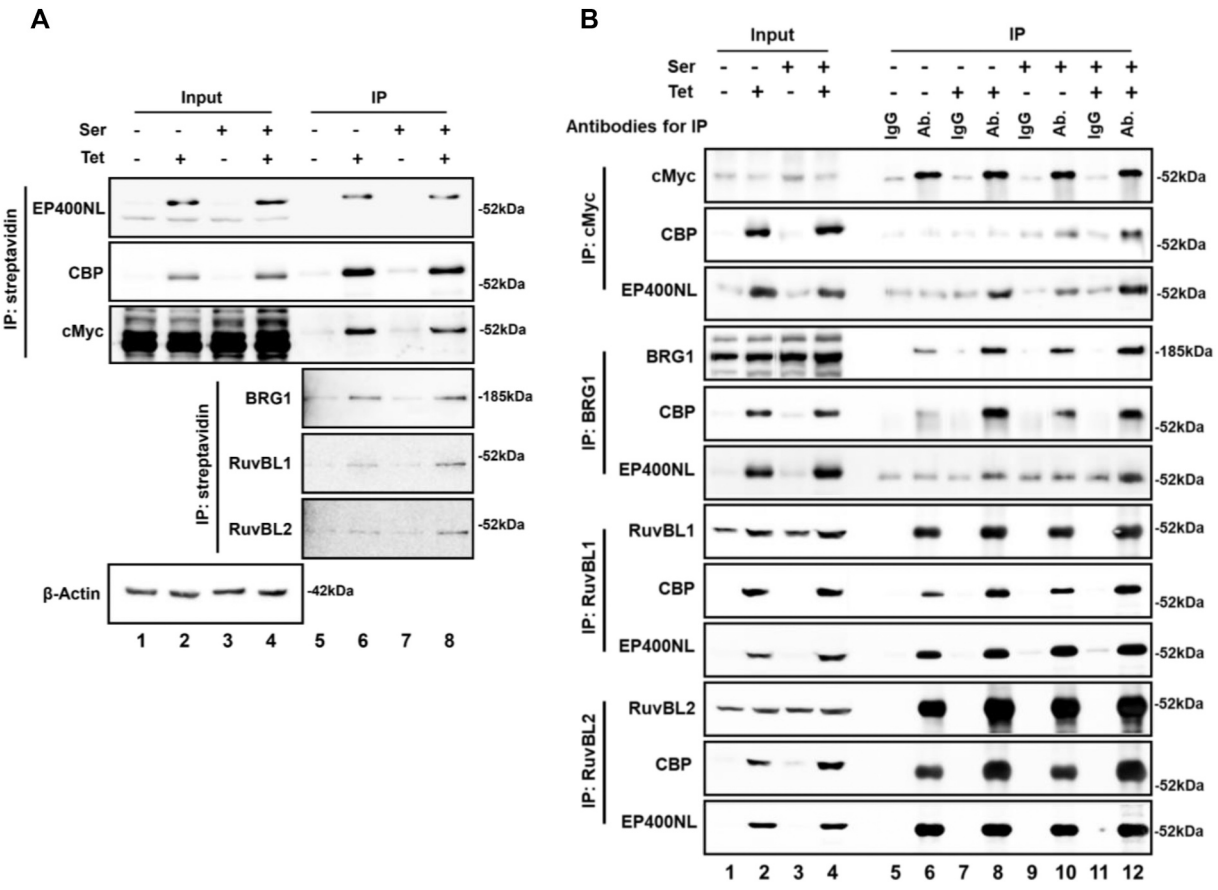

Fig. 6. EP400NL complex interacts with cMyc.
(A) Co-immunoprecipitation experiments for the protein-protein interaction of EP400NL, cMyc, BRG1, RuvBL1, and RuvBL2. EP400NL protein complexes were precipitated by streptavidin beads followed by the validation of both anti-EP400NL and anti-CBP immunoblots. The co-precipitations of cMyc, BRG1, RuvBL1, and RuvBL2 were confirmed by the immunoblots. (B) Reverse co-immunoprecipitation experiments were performed with the same cell lysates in (A). Immunoprecipitates by anti-cMyc, anti-BRG1, anti-RuvBL1, and anti-RuvBL2 antibodies (Ab.) were examined by both anti-CBP and anti-EP400NL immunoblots.

absence of additional serum and IFNγ-stimulation, to avoid a universal upregulation of genes by serum and IFNγ [46]. Under these conditions, the majority of genes, including *PD-L1*, were not differentially expressed above 1.5-fold range (Fig. 8A). The 121 genes with over 1.5-fold upregulation were further analysed by gene ontology (Fig. 8B), which revealed upregulation of housekeeping functions such as mitochondrial translation. EP400NL-dependent upregulations of three target genes for mitochondrial ribosomal proteins (MRPL15, MRPL27, and MRPL54) were further verified in a different cell line (Supplementary Fig. 3). The mitochondrial ribosomes are well-known cMyc targets to promote cell proliferation, mitochondrial biogenesis, and cancer [47–50]. In addition, 34.9 % of EP400NL-responsive genes (p-value < 0.05) overlapped with cMyc-upregulated genes (accession number: GSE164926) (Fig. 8C) [30]. Consistent with this finding, H1299 cell lines with EP400NL indels showed slower cell proliferation and increased cell distribution in the G0/G1 cell cycle (Supplementary Fig. 4). Taken together, the results may suggest that EP400NL regulates the subset of Myc target genes that are important in cell proliferation.

4. Discussion

Here we have determined that EP400NL, previously thought to be a pseudogene, forms a chromatin-remodelling complex similar to the EP400 complex. EP400NL itself is not an ATPase but our studies demonstrate that it is a component of a nuclear multi-protein complex that can catalyse an ATP-dependent H2A.Z deposition. In addition, upregulation of EP400NL enhances not only the expression of *PD-L1* gene but also cMyc target genes involved in mitochondrial biogenesis.

EP400NL appears to form a variant complex similar to the TIP60-deficient EP400 complex but containing the BRG1 ATPase. The association of BRG1 with the EP400NL complex may be relatively weaker and transient as the amount of BRG1 co-purified by EP400NL is minimal compared to other shared core subunits of the complex. BRG1 ATPase contains a highly conserved bromodomain at the C-terminus, and it might confer a missing ATPase function to the EP400NL complex [51]. Interestingly, the BRG1-containing BAF complex is also known to play a role in H2A.Z deposition in embryonic stem cells but little is understood about its molecular mechanism [52]. It is tempting to speculate that the EP400NL complex is a carrier of BRG1 in certain genomic regions of H2A.Z deposition activity, however, the connection between BRG1 and EP400NL complex-mediated H2A.Z deposition and the coactivator function remains to be further elucidated.

Although the level of cMyc was not altered significantly by serum stimulation in the EP400NL inducible Flp-In™ T-Rex™ cells, serum stimulation in the presence of upregulated EP400NL enhanced cMyc binding to the *PD-L1* promoter. ChIP data shows that the recruitment of EP400NL to the target promoter requires the binding of DNA binding transcription factors such as cMyc or other unknown serum-stimulated factors at the promoter and seems to play a role in the stabilised DNA binding activity through the protein-protein interactions [53]. The co-immunoprecipitation studies of cMyc and components of the EP400NL complex and their co-enrichment at the cMyc binding site of the *PD-L1* promoter support the model that cMyc recruits epigenetic modifying complexes to the target gene promoters for transcriptional activation

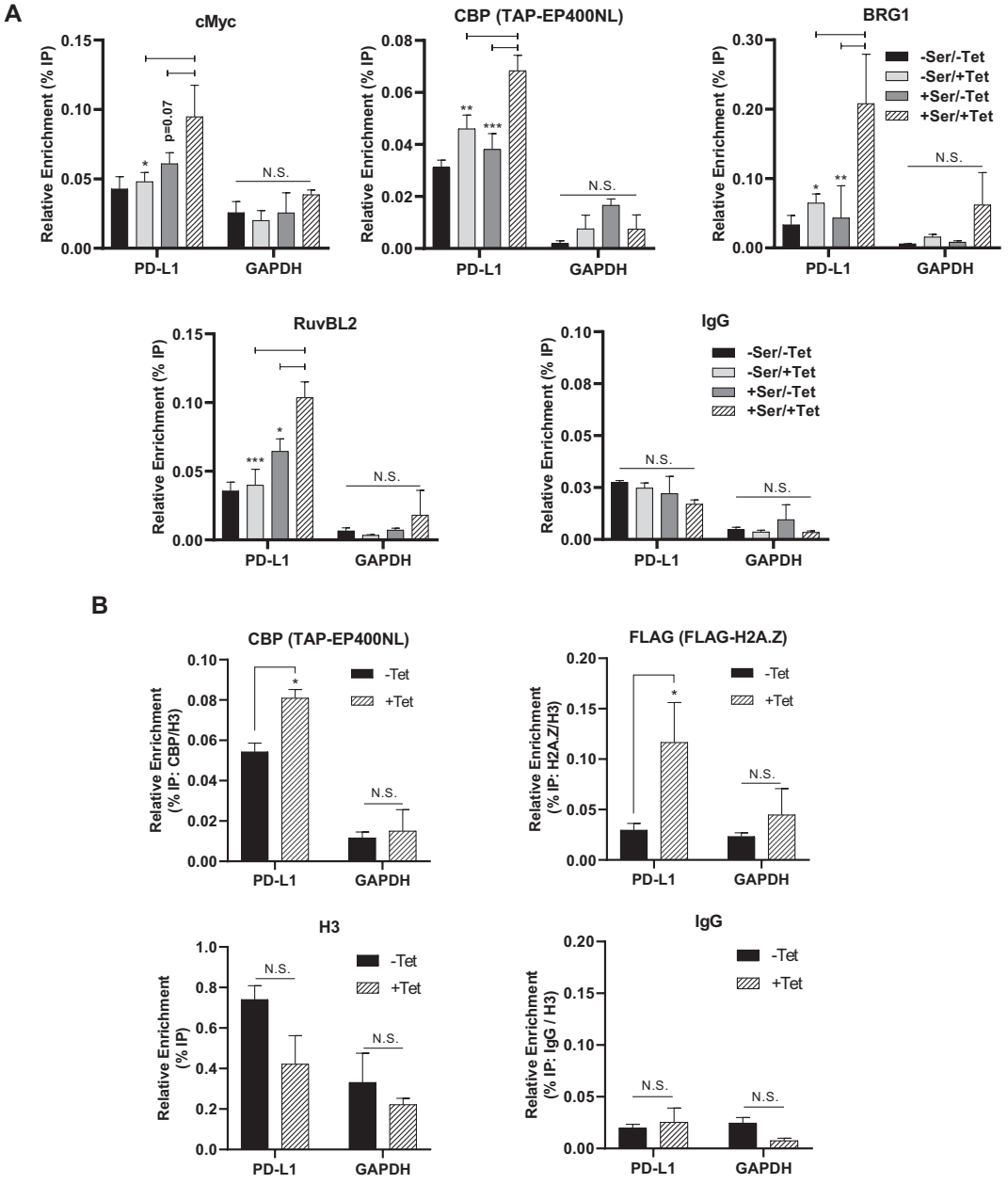

Fig. 7. EP400NL are recruited at the *PD-L1* promoter for transactivation.
(A) The enrichment of cMyc, EP400NL, BRG1, and RuvBL2 at the *PD-L1* promoter of Flp-In™ T-Rex™ cell line stably expressing tetracycline-inducible EP400NL. The purified DNA after ChIP reactions was analysed by qPCR over the regions of *PD-L1* promoter (Myc binding site) or GAPDH promoter. Four combinations of the experimental conditions (the presence and absence of serum and tetracycline: ±Ser/±Tet) were used in the ChIP analyses [Two-way ANOVA, $F_{(1,8)} = 36.01$, $p = 0.0003$ (cMyc), $F_{(1,8)} = 263.7$, $p < 0.0001$ (CBP), $F_{(1,8)} = 13.57$, $p = 0.0062$ (BRG1), $F_{(1,8)} = 103.6$, $p < 0.0001$ (RuvBL2); post-hoc Tukey's HSD, $^{*}p < 0.05$, $^{**}p < 0.01$, $^{***}p < 0.001$]. (B) In vivo enrichment of H2A.Z at the *PD-L1* promoter in Flp-In™ T-REx™ cell line that stably expressing tetracycline-inducible EP400NL. The purified DNA after ChIP reactions was analysed by qPCR over the regions of *PD-L1* promoter (Myc binding site) or GAPDH promoter. Two experimental conditions (the presence and absence of tetracycline: ±Tet) were used in the ChIP analyses under both serum and IFNγ stimulation [Two-way ANOVA, $F_{(1,4)} = 11.49$, $p = 0.0276$ (TAP-EP400NL), $F_{(1,4)} = 10.26$, $p = 0.0328$ (FLAG-H2A.Z); post-hoc Tukey's HSD, $^{*}p < 0.05$].

(Supplementary Fig. 5). Additionally, the PD-L1 expression pattern from cells with EP400NL indels suggests that EP400NL is required at an early stage of the transcriptional activation within 6 h of serum stimulation (Fig. 5A, left panel). PD-L1 overexpression is a predictor of recurrent cancer incidence and is associated with a poor prognosis in cancer patients [13,54]. Consistent with the role in the *PD-L1* gene regulation, cMyc expression correlates with PD-L1 expression in NSCLC [14]. In connection, a meta-analysis of mRNA expression profile identified EP400NL being upregulated in lung adenocarcinoma tissue from cancer patients who have a smoking history [55]. Multiple transcription factors and epigenetic protein complexes including the hNuA4, EP400, and BRG1-containing BAF complexes have been identified as interacting partners with cMyc to induce and maintain cancerous phenotypes [2,7,8,34,56–63]. Given that cMyc regulates ~15 % of all human genes, it is surprising to see only a small number of genes to be EP400NL responsive in our transcriptome analysis. Hence, the EP400NL complex is likely to be involved in a subset of cMyc functions such as immune evasion and mitochondrial biogenesis. cMyc is implicated in mitochondrial biogenesis through mitochondrial translation, protein import, and complex assembly [50]. It is not clear how cMyc-stimulated

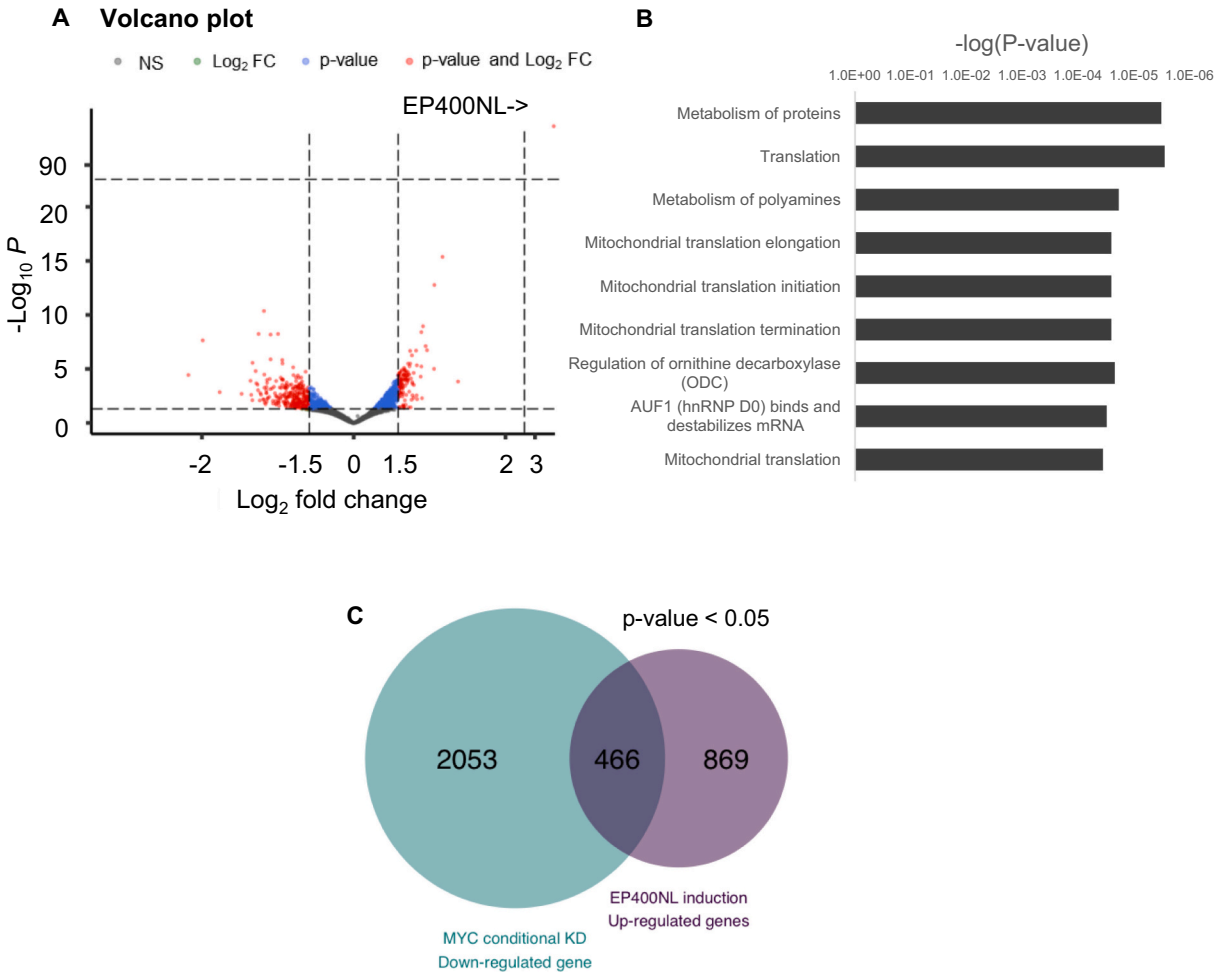

Fig. 8. EP400NL upregulates genes involved in mitochondrial biogenesis.
(A) RNA-seq volcano plot from tetracycline-induced TAP-EP400NL cell line differentially expressed from the non-induced cell line. Differentially expressed genes were indicated by red dots ($n = 20{,}398$, fold change > 1.5, p-value < 0.05). (B) Reactome pathway analysis for the up-regulated genes by EP400NL ($n = 122$, fold change > 1.5). (C) Venn diagram of EP400NL-responsive target genes ($p < 0.05$) overlapped with cMyc target genes (accession number: GSE164926). (For interpretation of the references to colour in this figure legend, the reader is referred to the web version of this article.)

mitochondrial biogenesis is implicated in cancer phenotypes but is thought to prepare cells for cell cycle entry. Downregulation of mitochondrial biogenesis would explain the slow cell growth and abnormal cell cycle distribution as observed in the EP400NL indels (Supplementary Fig. 4).

The importance of the PD-L1 pathway in advanced cancers has been demonstrated by impressive therapeutic success using antibody-based blockage of the immune evasion pathway in combination with conventional cancer therapies [10,11,64–67]. Given that cMyc plays a critical role in regulating immune evasion, a specific epigenetic regulator in Myc-dependent transcription might provide an opportunity to interfere with the immune evasion mechanism of cancer cells. Small-molecule agents that target epigenetic regulators have been shown to modulate PD-L1 expression levels via epigenetic modifications of *PD-L1* gene and induce various effects on the efficacy of anti-PD1/PD-L1 antibodies [68]. Future studies will explore whether the EP400NL-targeted incorporation of H2A.Z to the *PD-L1* promoter can modulate PD-L1 expression and its effects on the tumorigenic potential of cancer cells in animal models.

The exon regions of EP400NL are highly conserved across mammals, suggesting that the unique functions conferred by EP400NL may not be redundant with EP400. Otherwise, the redundant gene of the same function would have accumulated nonsynonymous mutations that cause a loss of function. Although we showed that EP400NL modifies serum- and IFNγ-mediated PD-L1 expression by forming a unique nuclear complex, the specific functional domains and direct binding partners of EP400NL remain to be identified. Therefore, elucidating the direct binding domain of EP400NL and recruitment of the interacting proteins into the complex will be a focus of future work. Furthermore, investigation of genome-wide ChIP-sequencing will provide better insight on how EP400NL contributes to human epigenome maintenance and gene regulation, especially in connection with cMyc-dependent cellular proliferation and oncogenic transformation.

Funding

This work was supported by a grant from Xi'an Jiaotong-Liverpool University Research Development Fund (RDF-20-01-13) to J.H.P., National Research Foundation of Korea (NRF-2018R1A5A1024261) to J. K., Massey University Doctoral Scholarship to Z.L.

CRediT authorship contribution statement

Jeong Park: Conceptualization, Data analysis, and Supervision. Zidong Li: Investigation, Data analysis, Original draft writing. Hyoungmin Kim: Investigation and Data analysis (Fig. 8). Jaehoon Kim: Data analysis and supervision. All authors contribute to write the original manuscript draft.

Declaration of competing interest

The authors declare that they have no known competing financial interests or personal relationships that could have appeared to influence the work reported in this paper.

Data availability

Tandem mass spectra from the mass spectrometric analysis of EP400NL nuclear complex were searched against the UniProt database of *Homo sapiens* (https://www.uniprot.org/proteomes/UP000005640), using Proteome Discoverer 2.2 (Thermo). The mass spectrometry proteomics data have been deposited to the ProteomeXchange Consortium via the PRIDE partner repository with the dataset identifier PXD026070.

Project Name

EP400NL is required for cMyc-mediated PD-L1 gene activation by forming a transcriptional coactivator complex.

Project accession

PXD026070.

Reviewer account details for peer review

Username: reviewer_pxd026070@ebi.ac.uk

Password: GL8AAzEg

The RNA expression data to identify EP400NL-responsive genes in Flp-In™ T-REx™ cells were submitted to GEO repository:

(GSE189729: https://www.ncbi.nlm.nih.gov/geo/query/acc.cgi?acc=GSE189729)

Acknowledgement

We thank Mr. Trevor Loo for his excellent technical support for mass spectrometric analysis. We acknowledge the Manawatu Microscopy and Imaging Centre for confocal microscopy use and their excellent technical assistance.

Appendix A. Supplementary data

Supplementary data to this article can be found online at https://doi.org/10.1016/j.bbagrm.2022.194889.

References

[1] Y. Doyon, W. Selleck, W.S. Lane, S. Tan, J. Cote, Structural and functional conservation of the NuA4 histone acetyltransferase complex from yeast to humans, Mol. Cell. Biol. 24 (2004) 1884–1896.
[2] H.Y. Yamada, Human Tip60 (NuA4) complex and cancer, in: R. Ettarh (Ed.), Colorectal Cancer Biology-From Genes to Tumor, Intechopen, 2012, pp. 217–240.
[3] P.Y.T. Lu, N. Levesque, M.S. Kobor, NuA4 and SWR1-C: two chromatin-modifying complexes with overlapping functions and components, Biochem. Cell Biol. 87 (2009) 799–815.
[4] Y. Xu, M.K. Ayrapetov, C. Xu, O. Gursoy-Yuzugullu, Y.D. Hu, B.D. Price, Histone H2A.Z controls a critical chromatin remodeling step required for DNA double-strand break repair, Mol. Cell 48 (2012) 723–733.
[5] S.K. Pradhan, T. Su, L.D. Yen, K. Jacquet, C. Huang, J. Cote, S.K. Kurdistani, M. F. Carey, Chromatin remodeler EP400 deposits H3.3 into promoters and enhancers during gene activation, Mol Cell 61 (2016) 27–38.
[6] B.D. Giaimo, F. Ferrante, A. Herchenrother, S.B. Hake, T. Borggrefe, The histone variant H2A.Z in gene regulation, Epigenetics Chromatin 12 (2019) 37, https://doi.org/10.1186/s13072-019-0274-9.
[7] K.A. Tworkowski, A.A. Chakraborty, A.V. Samuelson, Y.R. Seger, M. Narita, G. J. Hannon, S.W. Lowe, W.P. Tansey, Adenovirus E1A targets p400 to induce the cellular oncoprotein Myc, Proc. Natl. Acad. Sci. U. S. A. 105 (2008) 6103–6108.
[8] L.J. Zhao, P.M. Loewenstein, M. Green, Enhanced MYC association with the NuA4 histone acetyltransferase complex mediated by the adenovirus E1A N-terminal domain activates a subset of MYC target genes highly expressed in cancer cells, GenesCancer 8 (2017) 752–761.
[9] J. Park, S. Kunjibettu, S.B. McMahon, M.D. Cole, The ATM-related domain of TRRAP is required for histone acetyltransferase recruitment and Myc-dependent oncogenesis, Genes Dev. 15 (2001) 1619–1624.
[10] S. Gaikwad, M.Y. Agrawal, I. Kaushik, S. Ramachandran, S.K. Srivastava, Immune checkpoint proteins: signaling mechanisms and molecular interactions in cancer immunotherapy, Semin. Cancer Biol. 86 (2022) 137–150.
[11] X. He, C. Xu, Immune checkpoint signaling and cancer immunotherapy, Cell Res. 30 (2020) 660–669.
[12] X. Jiang, J. Wang, X. Deng, F. Xiong, J. Ge, B. Xiang, X. Wu, J. Ma, M. Zhou, X. Li, Y. Li, G. Li, W. Xiong, C. Guo, Z. Zeng, Role of the tumor microenvironment in PD-L1/PD-1-mediated tumor immune escape, Mol. Cancer 18 (2019) 10.
[13] S.C. Casey, L. Tong, Y.L. Li, R. Do, S. Walz, K.N. Fitzgerald, A.M. Gouw, V. Baylot, I. Gutgemann, M. Eilers, D.W. Felsher, MYC regulates the antitumor immune response through CD47 and PD-L1, Science 352 (2016) 227–231.
[14] E.Y. Kim, A. Kim, S.K. Kim, Y.S. Chang, MYC expression correlates with PD-L1 expression in non-small cell lung cancer, Lung Cancer 110 (2017) 63–67.
[15] N. Karachaliou, M. Gonzalez-Cao, G. Crespo, A. Drozdowskyj, E. Aldeguer, A. Gimenez-Capitan, C. Teixido, M.A. Molina-Vila, S. Viteri, M.D. Gil, S.M. Algarra, E. Perez-Ruiz, I. Marquez-Rodas, D. Rodriguez-Abreu, R. Blanco, T. Puertolas, M. A. Royo, R. Rosell, Interferon gamma, an important marker of response to immune checkpoint blockade in non-small cell lung cancer and melanoma patients, Ther. Adv. Med. Oncol. 10 (2018).
[16] B. Seliger, Basis of PD1/PD-L1 therapies, J. Clin. Med. 8 (2019) 2168, https://doi.org/10.3390/jcm8122168.
[17] X.L. Ju, H. Zhang, Z.D. Zhou, Q. Wang, Regulation of PD-L1 expression in cancer and clinical implications in immunotherapy, Am. J. Cancer Res. 10 (2020) 1–11.
[18] M.E. Keir, M.J. Butte, G.J. Freeman, A.H. Sharpel, PD-1 and its ligands in tolerance and immunity, Annu. Rev. Immunol. 26 (2008) 677–704.
[19] J. Chen, C.C. Jiang, L. Jin, X.D. Zhang, Regulation of PD-L1: a novel role of pro-survival signalling in cancer, Ann. Oncol. 27 (2016) 409–416.
[20] X.J. Jiang, J. Wang, X.Y. Deng, F. Xiong, J.S. Ge, B. Xiang, X. Wu, J. Ma, M. Zhou, X.L. Li, Y. Li, G.Y. Li, W. Xiong, C. Guo, Z.Y. Zeng, Role of the tumor microenvironment in PD-L1/PD-1-mediated tumor immune escape, Mol. Cancer 18 (2019) 10, https://doi.org/10.1186/s12943-018-0928-4.
[21] R.J. Smith, M.S. Savoian, L.E. Weber, J.H. Park, Ataxia telangiectasia mutated (ATM) interacts with p400 ATPase for an efficient DNA damage response, BMC Mol. Biol. 17 (2016) 22, https://doi.org/10.1186/s12867-016-0075-7.
[22] I.M. Slaymaker, L.Y. Gao, B. Zetsche, D.A. Scott, W.X. Yan, F. Zhang, Rationally engineered Cas9 nucleases with improved specificity, Science 351 (2016) 84–88.
[23] M.F. Carey, C.L. Peterson, S.T. Smale, Dignam and Roeder nuclear extract preparation, Cold Spring Harb. Protoc. 2009 (2009) pdb prot5330.
[24] K. Ghosh, M. Tang, N. Kumari, A. Nandy, S. Basu, D.P. Mall, K. Rai, D. Biswas, Positive regulation of transcription by human ZMYND8 through its association with P-TEFb complex, Cell Rep. 24 (2018) 2141–2154.
[25] D.W. Kufe, COMPOSITIONS AND METHODS OF TREATING CANCER, DANA-FARBER CANCER INSTITUTE, INC. (Boston, MA, US), United States, 2020.
[26] A.M. Bolger, M. Lohse, B. Usadel, Trimmomatic: a flexible trimmer for Illumina sequence data, Bioinformatics 30 (2014) 2114–2120.
[27] A. Dobin, C.A. Davis, F. Schlesinger, J. Drenkow, C. Zaleski, S. Jha, P. Batut, M. Chaisson, T.R. Gingeras, STAR: ultrafast universal RNA-seq aligner, Bioinformatics 29 (2013) 15–21.
[28] Y. Liao, G.K. Smyth, W. Shi, featureCounts: an efficient general purpose program for assigning sequence reads to genomic features, Bioinformatics 30 (2014) 923–930.
[29] M.I. Love, W. Huber, S. Anders, Moderated estimation of fold change and dispersion for RNA-seq data with DESeq2, Genome Biol. 15 (2014) 550, https://doi.org/10.1186/s13059-014-0550-8.
[30] C.M. Woodley, A.S. Romer, J. Wang, A.D. Guarnaccia, D.L. Elion, J.N. Maxwell, K. Guerrazzi, T.S. McCann, T.M. Popay, B.K. Matlock, D.K. Flaherty, S.L. Lorey, Q. Liu, W.P. Tansey, A.M. Weissmiller, Multiple interactions of the oncoprotein transcription factor MYC with the SWI/SNF chromatin remodeler, Oncogene 40 (2021) 3593–3609.
[31] Y. Doyon, J. Cote, The highly conserved and multifunctional NuA4 HAT complex, Curr. Opin. Genet. Dev. 14 (2004) 147–154.
[32] A. Lopez-Perrote, H.E. Alatwi, E. Torreira, A. Ismail, S. Ayora, J.A. Downs, O. Llorca, Structure of Yin Yang 1 oligomers that cooperate with RuvBL1-RuvBL2 ATPases, J. Biol. Chem. 289 (2014) 22614–22629.
[33] G. Mizuguchi, X. Shen, J. Landry, W.H. Wu, S. Sen, C. Wu, ATP-driven exchange of histone H2AZ variant catalyzed by SWR1 chromatin remodeling complex, Science 303 (2004) 343–348.
[34] M. Fuchs, J. Gerber, R. Drapkin, S. Sif, T. Ikura, V. Ogryzko, W.S. Lane, Y. Nakatani, D.M. Livingston, The p400 complex is an essential E1A transformation target, Cell 106 (2001) 297–307.
[35] B. Stielow, A. Sapetschnig, C. Wink, I. Kruger, G. Suske, SUMO-modified Sp3 represses transcription by provoking local heterochromatic gene silencing, EMBO Rep. 9 (2008) 899–906.
[36] J. Haas, D. Bloesel, S. Bacher, M. Kracht, M.L. Schmitz, Chromatin targeting of HIPK2 leads to acetylation-dependent chromatin decondensation, Front. Cell Dev. Biol. 8 (2020) 852, https://doi.org/10.3389/fcell.2020.00852.
[37] M. Tufano, P. D'Arrigo, M. D'Agostino, C. Giordano, L. Marrone, E. Cesaro, M. F. Romano, S. Romano, PD-L1 expression fluctuates concurrently with cyclin D in glioblastoma cells, Cells 10 (2021) 2366, https://doi.org/10.3390/cells10092366.
[38] S. Xue, M. Hu, P. Li, J. Ma, L. Xie, F. Teng, Y. Zhu, B. Fan, D. Mu, J. Yu, Relationship between expression of PD-L1 and tumor angiogenesis, proliferation, and invasion in glioma, Oncotarget 8 (2017) 49702–49712.
[39] E.A. Akbay, S. Koyama, J. Carretero, A. Altabef, J.H. Tchaicha, C.L. Christensen, O. R. Mikse, A.D. Cherniack, E.M. Beauchamp, T.J. Pugh, M.D. Wilkerson, P.E. Fecci, M. Butaney, J.B. Reibel, M. Soucheray, T.J. Cohoon, P.A. Janne, M. Meyerson, D. N. Hayes, G.I. Shapiro, T. Shimamura, L.M. Sholl, S.J. Rodig, G.J. Freeman, P. S. Hammerman, G. Dranoff, K.K. Wong, Activation of the PD-1 pathway contributes to immune escape in EGFR-driven lung tumors, Cancer Discov. 3 (2013) 1355–1363.

[40] F. Antonangeli, A. Natalini, M.C. Garassino, A. Sica, A. Santoni, F. Di Rosa, Regulation of PD-L1 expression by NF-kappa B in cancer, Front. Immunol. 11 (2020) 584626.
[41] A. Garcia-Diaz, D.S. Shin, B.H. Moreno, J. Saco, H. Escuin-Ordinas, G.A. Rodriguez, J.M. Zaretsky, L. Sun, W. Hugo, X.Y. Wang, G. Parisi, C.P. Saus, D.Y. Torrejon, T. G. Graeber, B. Comin-Anduix, S. Hu-Lieskovan, R. Damoiseaux, R.S. Lo, A. Ribas, Interferon receptor signaling pathways regulating PD-L1 and PD-L2 expression (vol 19, pg 1189, Cell Rep. 19 (2017) 1189–1201.
[42] K. Gowrishankar, D. Gunatilake, S. Gallagher, J. Tiffen, P. Hersey, Regulation of PD-L1 expression in human melanoma by NF-kappa B, Cancer Res. 74 (19) (2014) 2947.
[43] K.J. Lastwika, W. Wilson, Q.K. Li, J. Norris, H.Y. Xu, S.R. Ghazarian, H. Kitagawa, S. Kawabata, J.M. Taube, S. Yao, L.N. Liu, J.J. Gills, P.A. Dennis, Control of PD-L1 expression by oncogenic activation of the AKT-mTOR pathway in non-small cell lung cancer, Cancer Res. 76 (2016) 227–238.
[44] J.W. Moon, S.K. Kong, B.S. Kim, H.J. Kim, H. Lim, K. Noh, Y. Kim, J.W. Choi, J. H. Lee, Y.S. Kim, IFN gamma induces PD-L1 overexpression by JAK2/STAT1/IRF-1 signaling in EBV-positive gastric carcinoma, Sci. Rep.-UK 7 (1) (2017) 17810.
[45] Y. Wang, J.Z. Hu, Y.A. Wang, W.M. Ye, X.K. Zhang, H.Y. Ju, D.L. Xu, L. Liu, D. X. Ye, L. Zhang, D.W. Zhu, J. Deng, Z.Y. Zhang, S.L. Liu, EGFR activation induced snail-dependent EMT and myc-dependent PD-L1 in human salivary adenoid cystic carcinoma cells, Cell Cycle 17 (2018) 1457–1470.
[46] Z. Nie, G. Hu, G. Wei, K. Cui, A. Yamane, W. Resch, R. Wang, D.R. Green, L. Tessarollo, R. Casellas, K. Zhao, D. Levens, c-Myc is a universal amplifier of expressed genes in lymphocytes and embryonic stem cells, Cell 151 (2012) 68–79.
[47] G. Huang, H. Li, H. Zhang, Abnormal expression of mitochondrial ribosomal proteins and their encoding genes with cell apoptosis and diseases, Int. J. Mol. Sci. 21 (22) (2020) 8879.
[48] S. Bao, X. Wang, M. Li, Z. Gao, D. Zheng, D. Shen, L. Liu, Potential of mitochondrial ribosomal genes as cancer biomarkers demonstrated by bioinformatics results, Front. Oncol. 12 (2022), 835549.
[49] S. Vyas, E. Zaganjor, M.C. Haigis, Mitochondria and cancer, Cell 166 (2016) 555–566.
[50] F. Morrish, D. Hockenbery, MYC and mitochondrial biogenesis, Cold Spring Harb. Perspect. Med. 4 (5) (2014) a014225.
[51] J.C. Sanchez, L.Y. Zhang, S. Evoli, N.J. Schnicker, M. Nunez-Hernandez, L.P. Yu, J. Wereszczynski, M.A. Pufall, C.A. Musselman, The molecular basis of selective DNA binding by the BRG1 AT-hook and bromodomain, BBA-Gene Regul. Mech. 1863 (8) (2020) 194566.
[52] S.J. Hainer, T.G. Fazzio, Regulation of nucleosome architecture and factor binding revealed by nuclease footprinting of the ESC genome, Cell Rep. 13 (2015) 61–69.
[53] Z. Wang, P. Wang, Y. Li, H. Peng, Y. Zhu, N. Mohandas, J. Liu, Interplay between cofactors and transcription factors in hematopoiesis and hematological malignancies, Signal Transduct. Target. Ther. 6 (2021) 24.
[54] X. Wang, F.F. Teng, L. Kong, J.M. Yu, PD-L1 expression in human cancers and its association with clinical outcomes, Oncotargets Ther. 9 (2016) 5023–5039.
[55] X.N. He, C. Zhang, C. Shi, Q.Q. Lu, Meta-analysis of mRNA expression profiles to identify differentially expressed genes in lung adenocarcinoma tissue from smokers and non-smokers, Oncol. Rep. 39 (2018) 929–938.
[56] S.B. McMahon, H.A. Van Buskirk, K.A. Dugan, T.D. Copeland, M.D. Cole, The novel ATM-related protein TRRAP is an essential cofactor for the c-Myc and E2F oncoproteins, Cell 94 (1998) 363–374.
[57] J. Park, S. Kunjibettu, S.B. McMahon, M.D. Cole, The ATM-related domain of TRRAP is required for histone acetyltransferase recruitment and Myc-dependent oncogenesis, Gene Dev. 15 (2001) 1619–1624.
[58] M.A. Nikiforov, S. Chandriani, J. Park, I. Kotenko, D. Matheos, A. Johnsson, S. B. McMahon, M.D. Cole, TRRAP-dependent and TRRAP-independent transcriptional activation by Myc family oncoproteins, Mol. Cell. Biol. 22 (2002) 5054–5063.
[59] J. Park, M.A. Wood, M.D. Cole, BAF53 forms distinct nuclear complexes and functions as a critical c-Myc-interacting nuclear cofactor for oncogenic transformation, Mol. Cell. Biol. 22 (2002) 1307–1316.
[60] S.R. Frank, T. Parisi, S. Taubert, P. Fernandez, M. Fuchs, H.M. Chan, D. M. Livingston, B. Amati, MYC recruits the TIP60 histone acetyltransferase complex to chromatin, EMBO Rep. 4 (2003) 575–580.
[61] X.H. Liu, J. Tesfai, Y.A. Evrard, S.Y.R. Dent, E. Martinez, C-Myc transformation domain recruits the human STAGA complex and requires TRRAP and GCN5 acetylase activity for transcription activation, J. Biol. Chem. 278 (2003) 20405–20412.
[62] V.H. Cowling, M.D. Cole, Mechanism of transcriptional activation by the Myc oncoproteins, Semin. Cancer Biol. 16 (2006) 242–252.
[63] M. Vita, M. Henriksson, The Myc oncoprotein as a therapeutic target for human cancer, Semin. Cancer Biol. 16 (2006) 318–330.
[64] J. Gong, A. Chehrazi-Raffle, S. Reddi, R. Salgia, Development of PD-1 and PD-L1 inhibitors as a form of cancer immunotherapy: a comprehensive review of registration trials and future considerations, J. Immunother. Cancer 6 (1) (2018) 8.
[65] Y. Guo, Progress in monoclonal antibody-based immunotherapy for cancer treatment, Sheng Wu Gong Cheng Xue Bao 31 (2015) 857–870.
[66] D.M. Pardoll, The blockade of immune checkpoints in cancer immunotherapy, Nat. Rev. Cancer 12 (2012) 252–264.
[67] L.M. Weiner, J.C. Murray, C.W. Shuptrine, Antibody-based immunotherapy of cancer, Cell 148 (2012) 1081–1084.
[68] H. Yamaguchi, J.M. Hsu, W.H. Yang, M.C. Hung, Mechanisms regulating PD-L1 expression in cancers and associated opportunities for novel small-molecule therapeutics, Nat. Rev. Clin. Oncol. 19 (2022) 287–305.